Analysis of failure mechanisms of Oxide - Oxide ceramic matrix composites

Ramachandran, K., Leelavinodhan, S., Antao, C., Copti, A., Mauricio, C., Jyothi, Y. L. & Jayaseelan, D. D

DOI 10.1016/j.jeurceramsoc.2021.11.020
ISSN 0955-2219

Publisher: Elsevier

Authors would like to thank Dr Anish Paul, Ansaldo Energia, Switzerland for providing oxide CMC samples for research. The authors acknowledge the support of Mr. Dean Wells and Mr. Alex Vine from Kingston University, London and Mr. Collin Small and Mr. Martin Bache from Swansea University for their assistance offered towards mechanical testing. One of the authors, Karthikeyan would like to acknowledge the support provided by Kingston University, London for the studentship towards his PhD research

Journal of the European Ceramic Society 42 (2022) 1626–1634

Contents lists available at ScienceDirect

Journal of the European Ceramic Society

journal homepage: www.elsevier.com/locate/jeurceramsoc

Analysis of failure mechanisms of Oxide - Oxide ceramic matrix composites

Karthikeyan Ramachandran, Subhashree Leelavinodhan, Christian Antao, Antony Copti, Cantalapiedra Mauricio, Yelisetti Lakshmi Jyothi, Doni Daniel Jayaseelan *

Department of Aerospace and Aircraft Engineering, Kingston University, Roehampton Vale Campus, London, SW15 3DW, United Kingdom

ARTICLE INFO

Keywords:
Ceramic matrix composites
Failure mechanisms
Tensile behaviour
Fatigue behaviour
High temperature testing
Finite element analysis

ABSTRACT

The failure mechanisms of Oxide-Oxide ceramic matrix composites AS-N610 were studied at both room temperature and high temperature using tensile and fatigue tests with and without lateral and laminar notches. The unnotched coupons had an average tensile strength of 423 MPa with elastic modulus of 97 GPa at room temperature showing a perfect elastic behaviour whereas the laminar notched samples shown similar strength of 425 MPa with elastic modulus (98 GPa) revealing pseudo-ductile behaviour. A reduction in tensile strength of the oxide ceramic matrix composites was observed at high temperatures. Thermal shock experiments revealed that the retained strength of the samples quenched from 1100 °C deteriorated by ~10 % (395 ± 15 MPa). In all samples, fracture origin was observed on the mid-plane showing a higher degree of fiber pull-out, delamination and pseudo ductile behaviour. Finite element analysis confirmed higher stress concentration on the areas of failures.

1. Introduction

Composite materials have played a crucial role in the development of automobile, aerospace and military applications. With years of research, the composite materials have shown significant improvement in various fields in quality and performance levels with widespread applications. Weight reduction using composites on many applications have been extensively researched along with its stability in extreme environments [1]. Particularly, Ceramic matrix composites (CMCs) are among the advanced materials that are identified to be a potential candidate in field of aerospace and gas turbine industries for improving the trust to weight ratio [2,3]. CMCs are also considered for high temperature applications including rotating and static components such as such as nozzles, jet engines, heat shields and braking systems owing to its properties [4,5]. As CMCs could retain their thermo-mechanical properties even at very high temperature, they are promising and suitable replacement for its usage in high temperature applications [6].

While the use of non-oxide CMCs including SiC/SiC and C-based CMCs are limited due to their oxidative instability, the research towards oxide CMCs is increasing to overcome the limit of application temperatures [7]. Oxide-Oxide CMCs are made from oxide-based fibres and matrix having good oxidation resistance, corrosion resistance and low dielectric constants which makes them the potential candidates for higher service life applications like hot gas filters and exhaust components [8,9]. Even though oxide-oxide CMCs have better oxidation resistance and service life, some researchers provided evidence that the service life of certain oxide CMCs is shortened at temperature of 1000°C [10,11]. The alumina oxide-based CMCs have reduced creep resistance than the non-oxide CMCs due to the predominant ionic bond, so the creep study on the material is quite necessary to predict service life of material under high temperature [10]. Many other notable works have been conducted on the failure mechanism of CMCs such as matrix cracking and delamination in continuous fiber-based CMCs [12,13]. Kastritseas et al. studied the matrix cracking in the Nicalon/calcium aluminosilicate CMCs after thermal shock and proposed matrix cracking in cross-ply was the reason for crack initiation [14]. Likewise, the CMCs reinforced with Nextel™610 exhibited high strength and stiffness [15, 16]. However, owing to fine grain structure, CMC is sensitive to grain growth and creep [17]. Also, several studies have shown that the quasi-plastic behaviour of CMCs is due to weak bonding which led to crack deflection and fiber pull-out [1]. Even though for the past two decades extensive studies have been devoted to understanding the failure mechanism, the studies did not provide enough description on the damage on fatigue assessments and failures due to thermal cycling.

The present study focuses on the analysis of failure behaviour of oxide-oxide CMCs (AS-N610) by studying their mechanical behaviour at ambient and high temperatures. Further, the effect of pre-manufactured notches on tensile and fatigue behaviour of the CMCs has been

* Corresponding author.
E-mail address: d.daniel@kingston.ac.uk (D.D. Jayaseelan).

https://doi.org/10.1016/j.jeurceramsoc.2021.11.020
Received 2 August 2021; Received in revised form 3 November 2021; Accepted 9 November 2021
Available online 13 November 2021

Table 1
Material Description of AS-N610 Oxide CMCs.

Material	Density g/cm^3	Nominal Fibre Volume (%)	Nominal Matrix volume (%)	Open Porosity (%)	Thermal expansion (10^{-6}/°C)	Maximum expansion temperature (°C)
AS-N610	2.83	51	49	25	8.0	1000

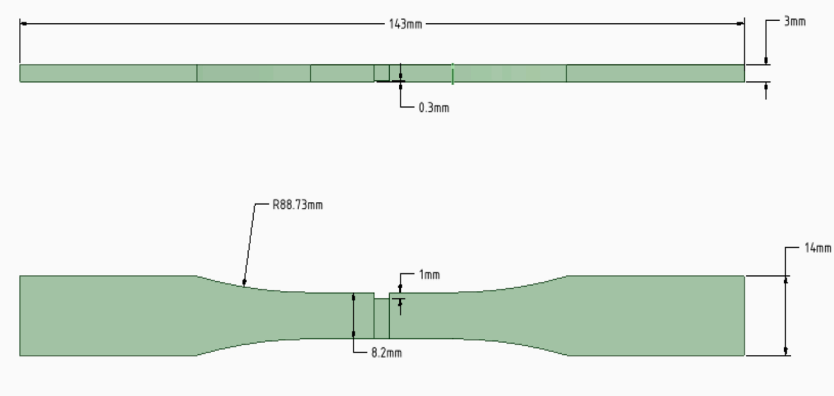

Fig. 1. Laminar and Lateral Notch on the CMC samples designed in Solidworks software.

investigated with same condition and the results are validated using finite element software Ansys 18.1.

2. Materials and methods

2.1. Material

Commercially available oxide-oxide CMCs designated as AS-N610, which was manufactured by COI ceramics, CA and consisted of continuous woven layers of Nextel™610 fibres in aluminosilicate matrix with a fibre orientation of 0 °/90 ° was used in this study. The properties of the oxide CMCs are given in Table 1. The desired oxide-oxide CMCs are manufactured using infiltration of the matrix precursor of aluminosilicate by sol-gel technique followed by vacuum bagging technique along with pressureless sintering. The oxide CMCs were commercially obtained (obtained from Ansaldo Energia, Italy) in the form of plate with dimensions 300 × 300 × 3 mm. The dog bone shaped coupons of dimension of 143 × 14 × 3 mm was machined out using waterjet cutting (Custom waterjet cutting Ltd. Uxbridge).

Laminar and lateral notches were introduced into the CMC samples using vertical milling machine as shown in Fig. 1. The notches were made in such a way that the laminar notch was 10 % of the thickness of CMC sample (0.3 mm deep and 3 mm long) and lateral notch was 12 % of width (1 mm wide and 3 mm in length) in mid-section of sample. The objective of the notches was to model the damage and analyse the failure on the samples that could occur during service conditions.

2.2. Testing methods

Room temperature tensile testing was carried out using Zwick/Roell Z050 universal testing machine (UTM) (Maximum applicable load: 50 K N) with help of epsilon extensometer as per ASTM C1359−11 [18]. The dog-bone shaped samples had end grips of 25 mm on each side using hydraulic wedges. The speed of the tensile testing was set to 1 mm/min until the failure of the samples. Instron 3300 with MTS 647 hydraulic wedges and 653 furnaces at Swansea university were used for the high temperature tensile studies. High temperature tensile testing was conducted at 900 °C, 1000 °C and 1100 °C with heating rate of 10 °C/min for the unnotched samples. The samples were inserted inside the furnace which is attached to UTM and held for 30 min at the desired testing

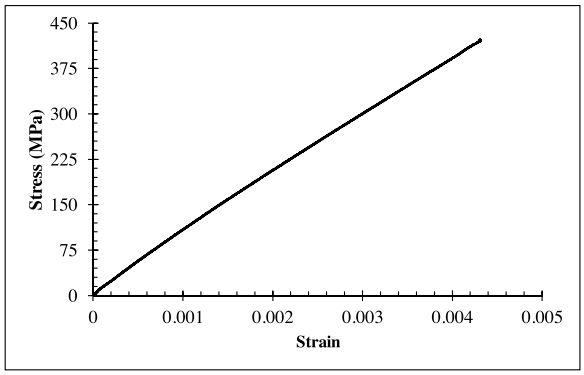

Fig. 2. Stress-Strain Curves of Oxide-Oxide CMCs in Room temperature.

temperatures and later testing was carried out with a ceramic arm displacement-controlled extensometer with gauge length of 25 mm. Finite element analysis using Ansys 18.1 was employed to validate the results obtained through experimental techniques for room temperature and high temperature tensile test using Von-Mises criteria to evaluate the equivalent stress [19]. Further, to study the behaviour of the notched samples under the influence of temperature, finite element model was employed. Fatigue tests were performed on unnotched and double notched specimens in the ambient environment. The test was carried out using Zwick/Roell AMSLER HC 25 fatigue testing machine. The fatigue test was carried out with frequency of 10 Hz with stress ratio of R= -1. The test was performed either to failure or to endure for 1 million cycles. One million cycles were chosen in assumption based on the maximum operating condition in a gas turbine which could accumulate total of 30−60 h in their lifetime [20]. The maximum stress for the different fatigue was set to 60 % of the ultimate tensile strength obtained for the CMCs though ambient tensile testing. Single cycle thermal shock was carried out for the oxide CMC samples at three different temperatures between 900−1100°C to understand the effect of thermal stress on the surface of CMCs after heat treatment process. The samples were heated in a box furnace with the heating rate of 10°C/min until the required temperature with dwell time of 1 h and quenched in air for 24 h prior to analyse the retained tensile strength.

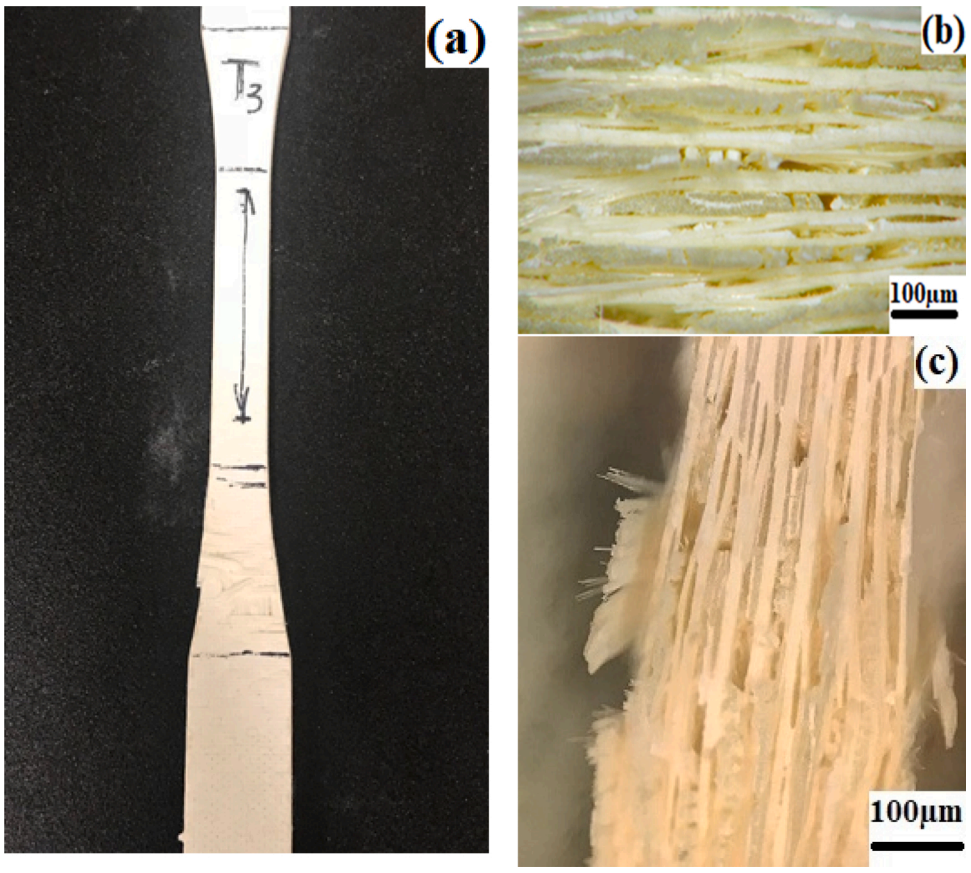

Fig. 3. (a) Samples after tensile test at room temperature (b) Fibre fracture occurring at neck region and (c) Fibre debonding from the matrix.

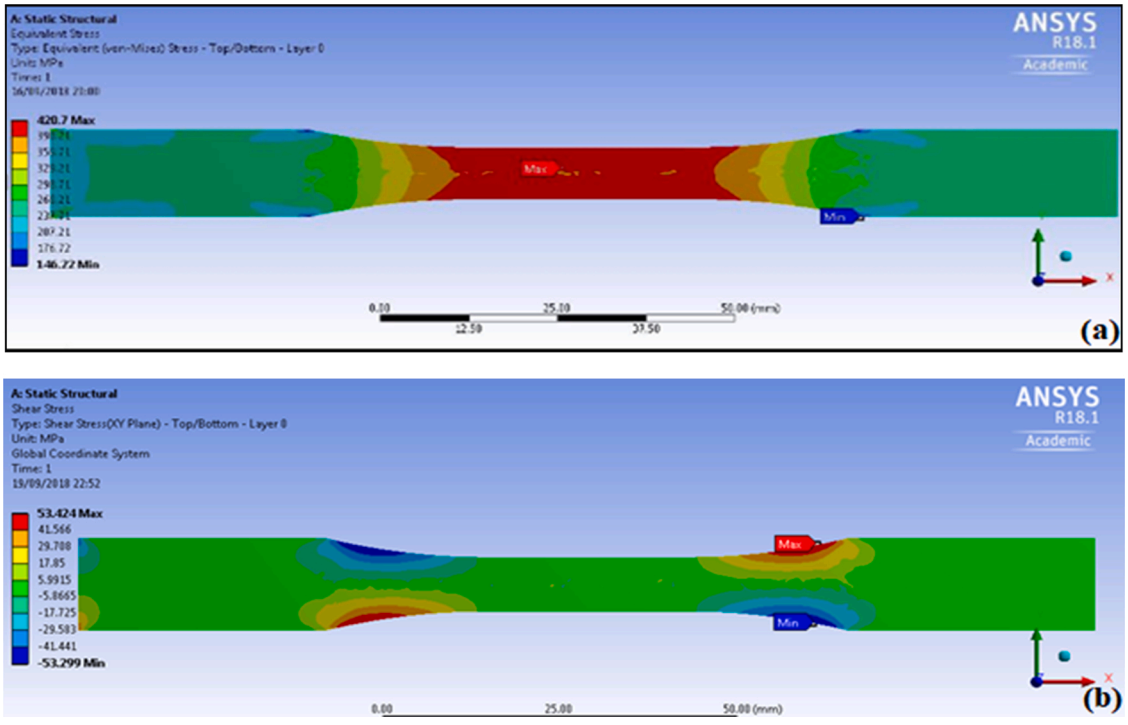

Fig. 4. (a) Stress distribution of oxide-oxide composite (b) Shear stress concentration on neck region of sample.

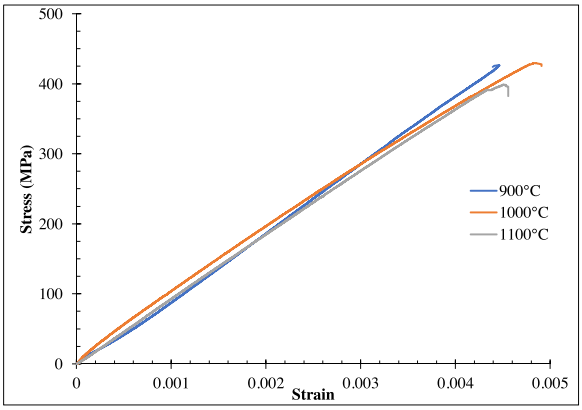

Fig. 5. Stress-Strain curve of oxide CMC samples after 1 -h thermal quenching.

3. Results and discussion

3.1. Room temperature tensile behaviour

Fig. 2 shows the stress-strain curve of Oxide-Oxide CMCs obtained for room temperature tensile testing with the help of extensometer. The uniaxial stress-strain graph reveals that a mean ultimate strength of 420 MPa was obtained with measured (computerised) elastic modulus of 97 GPa. From Fig. 2, the Elastic Modulus at room temperature at strain value 0.004 is 393/0.004 = 98.2 GPa. The tensile strength was noted to be higher compared with the data from previous studies and also CMC exhibited linear elastic behaviour at 0 °/90 ° layer similar to previous studies [21,22]. This dominating linear elastic behaviour could have been due to the 0 ° fibre lay ups which limited the matrix cracking and attributed towards additional delamination which resulted in higher tensile strength. The optical microscopic image shown in Fig. 3 of samples shown the fracture was not in the middle region as in most conventional materials under dog-bone shape rather the fracture occurred on the neck region (Fig. 3(a)). The area of fracture was similar in all the CMCs trails which could be action of the load acting along the direction of fibre alignment. The elongation on the samples after tensile testing provided evidence of fibre fracture and debonding along the loading area with significant fibre pull-out from the matrix as shown in Fig. 3(b & c). While analysing the region of failure on the samples, it can be said that the failures were attributed to the fibre debonding and pull-out which occurred on the CMCs along the fibre alignment direction. Further, due to the porous nature of the CMC sample, the fibre dominated the lay-up of the CMC rather than the matrix which provides a conclusive evidence of the role of fibre on the fracture mechanism.

A computational approach was designed to validate and predict failures occurring on the CMC samples using Ansys 18.1. The schematics of the model was like the experimental model of dog-bone shape utilised for study. The CMC laminate was designed using an FE modelling software Ansys with laminates consisting of homogenous layers at angles of 0 ° and 90 ° as provided by the manufacturer. Static structural analysis was utilised to validate the tensile strength. The orthogonal mechanical quality of 0.96 with mesh size of 1 mm and boundary conditions representing the real time experimental values where one side was fixed, and the other side was in tension with a displacement rate of 1 mm/min was considered in the analysis. The analysis was set to have the failure of the sample. The equivalent stress distribution at room temperature showing a maximum stress of 420 MPa occurring at the central region (Fig. 4(a)) of the sample was closer to result obtained via tensile strength obtained with help of extensometer (~423 MPa). The 10 % nominal difference between the experimental mean tensile strength and computational model could be neglected owing to the ambient operating temperature in the machining environment could change with machine temperature and surrounding environments. Also, the effect of induced porosity in the computational model had lesser impact owing to the morphology and alignment of CMC fibres in real time. Also, Fig. 4(b) shows the shear stress concentration on the neck region of the oxide-oxide samples which validate the area of two-piece fracture on the samples owing to shear stress acting along the aligned fibre direction.

Table 2
Retained tensile strength of oxide CMCs after thermal shock.

Temperature (°C)	Tensile Strength (MPa)	Elastic Modulus (GPa) (Computerised)
900	421 ± 10	96 ± 15
1000	428 ± 15	90 ± 15
1100	396 ± 15	87 ± 10

3.2. Thermal shock

Thermally shocked oxide CMC samples were quenched in air for 24 h before analysing the retained tensile strength. Fig. 5 shows the linear stress-strain curves of the tensile test for the samples quenched from three different temperatures. From the plotted curves, it can be seen that there is not much deterioration after the thermal shock for the samples tested at 900 °C and 1000 °C and they have the retained strength of ~420 MPa but 1100 °C had a slight deterioration of ~10 % compared to the room temperature tensile strength. From this Fig. 2, the elastic modulus at 0.004 strain value for 1100 °C thermal cycle samples is 87 GPa. The retained tensile strength and elastic modulus are plotted in Table 2.

The results obtained were compared with the data from COI ceramics and found that the material has an elastic modulus of 124 GPa at strain of 0.1 %. The Youngs modulus values of the composite were also calculated using the equations below.

Longitudinal Young's Modulus, E1

$$E_1 = E_f \cdot V_f + E_m \cdot V_m \quad (1)$$

E_f – *Young's modulus of fibre*
V_f – *Volume fraction of fibre*
E_m – *Young's modulus of matrix*
V_m – *Volume fraction of matrix*
$E_1 = 370\ GPa \times 0.51 + 87\ GPa \times 0.49$
$E_1 = 188.7\ GPa + 42.3\ GPa$
$E_1 = 231.3\ GPa$
Since the lay-up of the composite is 0/90, $E_1 = E_2$
Therefore, $\mathbf{E_1 = E_2 = 231.3\ GPa}$

Transverse Young's Modulus, E_3

$$\frac{1}{E_3} = \frac{V_m}{E_m} + \frac{V_f}{E_f} \quad (2)$$

$$\frac{1}{E_3} = \frac{0.49}{87\ GPa} + \frac{0.51}{370\ GPa}$$

$$\mathbf{E_3 = 142.6\ GPa}$$

The above calculation shows that the theoretical young's modulus is in range of 100–230 GPa for the oxide CMCs which is in comparison with the values provided by the COI ceramics. Based on the calculation from the stress-strain graph, 19 GPa was obtained as the modulus for the oxide CMCs at room temperature without extensometer, whereas with extensometer that has an average stress of 423 MPa at strain value of 0.004 resulted in 98 GPa which is in range to the data obtained from COI ceramics. Likewise, after thermal aging cycle, the samples quenched from 1100 °C has the elastic modulus of ~94 GPa which is also in comparison with the computerised values in this study. The results have been validated through ANSYS and it was found that the elastic modulus obtained at room temperature by tensile test was with 90 MPa which is again closer to theoretical and computerised data.

From Table 2 that the elastic modulus decreased with increase in

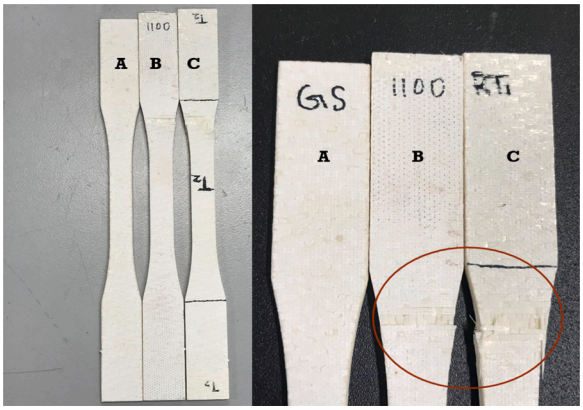

Fig. 6. Elongation and fracture on the oxide CMC samples at different conditions.

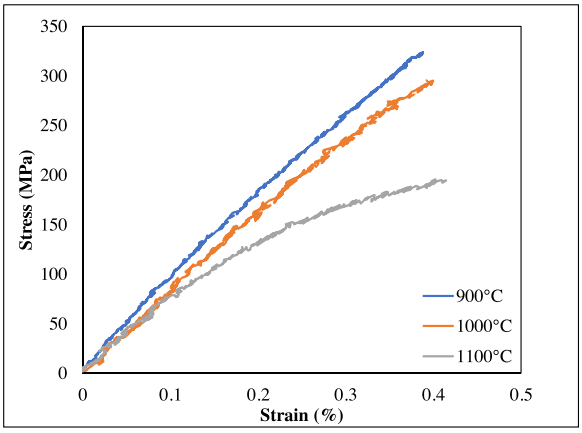

Fig. 7. Stress-Strain Curve of oxide CMCs at high temperature.

thermal shock temperature which could have been due to reduction in the mechanical stiffness and delamination. The damage in the oxide CMCs samples could have been due to the thermal stresses induced inside the porous matrix which led to material damage [23]. Many authors have studied the thermal shock induced damages and stated that the macroscopic cracks are caused by the micro-cracks in the matrix are induced by stresses during the shocks. However, most of the quenching techniques have been based on the water quenching technique which acts as sudden cool down mechanism which leads to formation of particles with same elemental analysis as matrix material along with micro-cracks and thermal damages [23,24]. But in this study, air quenching was carried out for 24 h which avoided most of the thermal induced cracks. Two different failure mechanisms were observed i.e., fibre pull-out and debonding of fibre and matrix. The fibre debonding is the dominated mechanism in thermal shock study which was further preceded by fibre pull-out mechanism as the fibre played major role in the CMC than the porous matrix. Fig. 6 shows the optical images of three different samples, A is non-tested coupon, B is the tensile tested coupon after thermal shock test at 1100 °C and C is the room temperature tensile tested coupon. Comparison of the elongation, coupon tensile tested at room temperature had large elongation than the thermally shocked samples which could have been due to the reduced elongation on the thermally shocked samples due to the release of thermal stresses. On the other hand, the fracture in B and C occurs on the same neck region with thermally shocked sample 1100 °C showing less elongation than the room temperature samples, and this is attributed to the maximum shear stress around that region which is confirmed by the FEA.

Table 3
Ambient & high temperature tensile properties of the oxide CMC samples.

Temperature (°C)	Tensile Strength (MPa) (Measured)	Equivalent stress through computational method	Elastic Modulus (GPa) (Computerised)
RT	423 ± 10	420.7	98 ± 15
900	323 ± 8	311.65	79 ± 15
1000	295 ± 5	270.05	70 ± 15
1100	195 ± 10	186.89	68 ± 15

3.3. High temperature tensile behaviour

Fig. 7 illustrates the stress-strain curves plotted for the oxide CMC samples at high temperatures (900, 1000 and 1100 °C). There is ~23% reduction of the tensile strength for the oxide CMCs at 900 °C. However, at 1000 °C, there is about ~30 % reduction in the tensile strength of oxide CMCs and ~53% for the sample at 1100 ° compared to room temperature samples. The tensile strength and the elastic modulus values are tabulated in Table 3. As the temperature increases, there is a significant drop in young's modulus and stiffness of the materials.

The tensile strength results of the oxide CMCs at higher temperature show that the thermo-mechanical stability of the CMCs at 1200 °C with no notable change in cross sectional area and strain. The way the CMCs fracture at high temperatures was similar to the room temperature fracture which occurred closer to the neck surface rather than the shoulder area of samples. The microscopic images revealed different fracture mechanisms including debonding, fibre bundle pull-out and matrix cracking. In high temperature environments when matrix cracks due to the thermal stresses on the surfaces of oxide CMCs is anticipated to be the leading fracture mechanism in temperature induced tensile testing. The occurrence of matrix cracks was less due to the porous nature of the oxide composites. However, stresses acting on the fibres reduced the load acting on the matrix by transmitting stress through sliding resistance into matrix and fibres. The fracture behaviour shows disoriented fibre pull-outs in the normal direction (Fig. 8) to the fibre reinforcement along with bundled pull-outs on the fibre direction. The shear stresses acting along the fibre direction are responsible for the fibre debonding along with fibre pull-out from the matrix. Also, thermal stresses induced on the matrix are released through the pores on the samples which reduce the effect of temperature on the matrix of the samples.

3.4. Fatigue behaviour

Ambient temperature fatigue testing was carried out with varying UTS (20–60 %) percentage was applied on the samples to estimate the fatigue life at room temperature. It was observed in Fig. 9 that with an increase in the percentage of UTS load, there was drop in number of cycles in the fatigue behaviour. The results show that the sample with 20 % UTS did not fail even after million cycles whereas with 60 % of UTS the samples were able to withstand only 35 cycles.

By comparing the failures of the samples tested after fatigue and tensile tests, the samples failed at shoulder region for both the tests with fatigue having lesser delamination. The optical microscopic observation of the fatigue tested samples revealed a larger amount of fibre pull-out (Fig. 10) occurring from the outer region towards the internal fibres. The magnitude of the longitudinal fibre pull-out varied based on the UTS from test to test with maximum pull-out length of 8 mm observed for 60 % UTS in fatigue test. This indicates that the damage on the samples could be acted on loading fatigue with early matrix cracking on the CMCs leading to bridging of fibres. The pre-existed porosity of the CMC material led to presence of cavities between matrix and fibres. Under fatigue loading conditions, there cavities acted as initiative for cracks by concentrating the stress from the unloading conditions leading to fibre buckling. These failure forms have been widely reported in previous

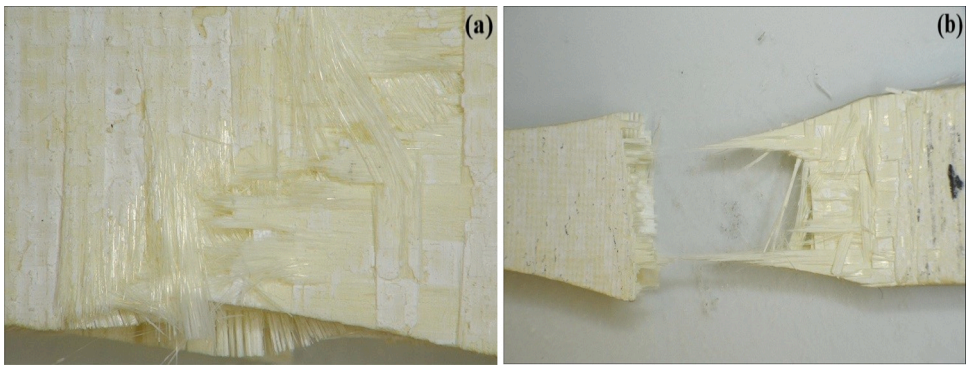

Fig. 8. (a) Disoriented Fibre pull-out in the normal direction to the fibre alignment and (b) Bundled fibre pull-out responsible for two-piece breakage.

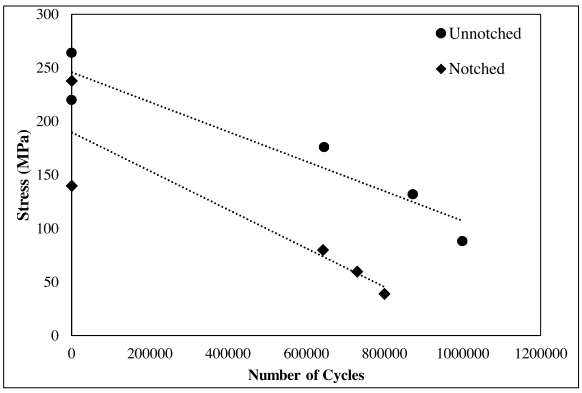

Fig. 9. S-N curve for unnotched and notched oxide CMC samples.

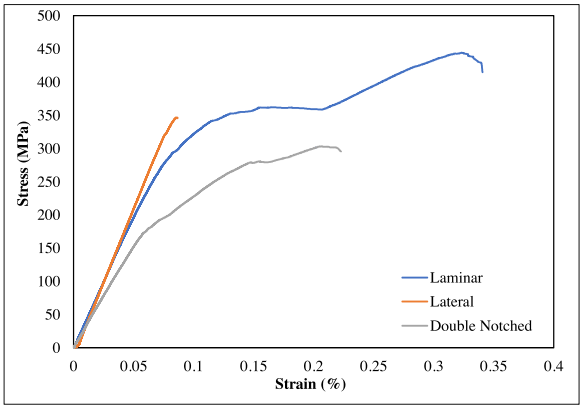

Fig. 11. Stress-Strain curve plotted for notched oxide CMC samples.

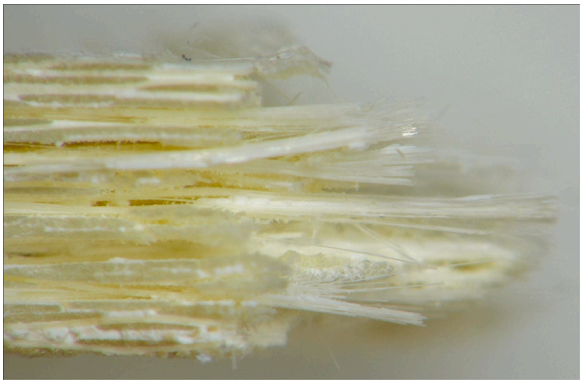

Fig. 10. Fibre pull-out mechanism observed at 60 % tensile strength on fatigue analysis.

studies [8,25].

3.5. Effect of notches

Ambient condition tensile and fatigue testing was carried out for the notched samples with same conditions of the unnotched samples. The room temperature tensile test was carried out for three samples (Laminar notch, lateral and double notch) with displacement speed of 1 mm/min and stress-strain curve was plotted in Fig. 11.

By observing the stress-strain curves plotted in Fig. 11, the mean strength of laminar notched sample was 429 MPa with elastic modulus of 98 GPa whereas the lateral represented a strength of 346 MPa with elastic modulus of 102 GPa and double notched samples had 297 MPa where the strain were measured using computerised technique. By comparing the results of notched and unnotched samples, the laminar notched samples did not have any reduction in strength whereas lateral and double notched samples shown deterioration of ~20 % and ~30 %. However, the elastic modulus of the laminar notch sample was closer to unnotched samples, the modulus of lateral (102 GPa) and double notches (119 GPa) increased by 3% and 20 %. From graph, laminar notched samples shown a non-linear plot representing a pseudo-ductile behaviour. From optical macroscopic Fig. 12(a – c), the laminar notched samples show a twisting effect caused by the formation of shear stress which results in coupling of longitudinal and twist stresses. The pseudo ductile behaviour of the CMCs could be responsible for the formation of shear stress which might leads to matrix crack initiation leading to further damage [26,27].

The further analysis of laminar notched samples shows that the failure mechanism was dominated by delamination which was observed on the first layer and bottom layers of the samples. The fibre failure was observed to be occurred on the parallel plane (~25 mm away) from the mid plane due to the shear stress. The formation of shear stress might be dependent on the orthotropic behaviour of the composite material which could change the tensile stress into shear stress which causes twisting momentum [28]. The laminar notched samples also shown certain fibre pull-out mechanism occurring away from the tensile stress direction which could have been a cause of misalignment between force and body axis leading to matrix cracking and debonding mechanism which could allow the fibre to move freely until its failure [25,28]. Whereas in lateral and double notched samples, the sudden breakage in the stress-strain graph along with perfect elastic behaviour could lead to a conclusive brittle behaviour. The perfect elastic behaviour and brittle failure could be due to interfacing debonding and multi-axial loading on the fibres which could deactivate the fibre pull-out in the sample leading to sudden breakage. Zhang et al. reported that owing to transverse or shear stress and critical values lead the fibre undergo instantaneous

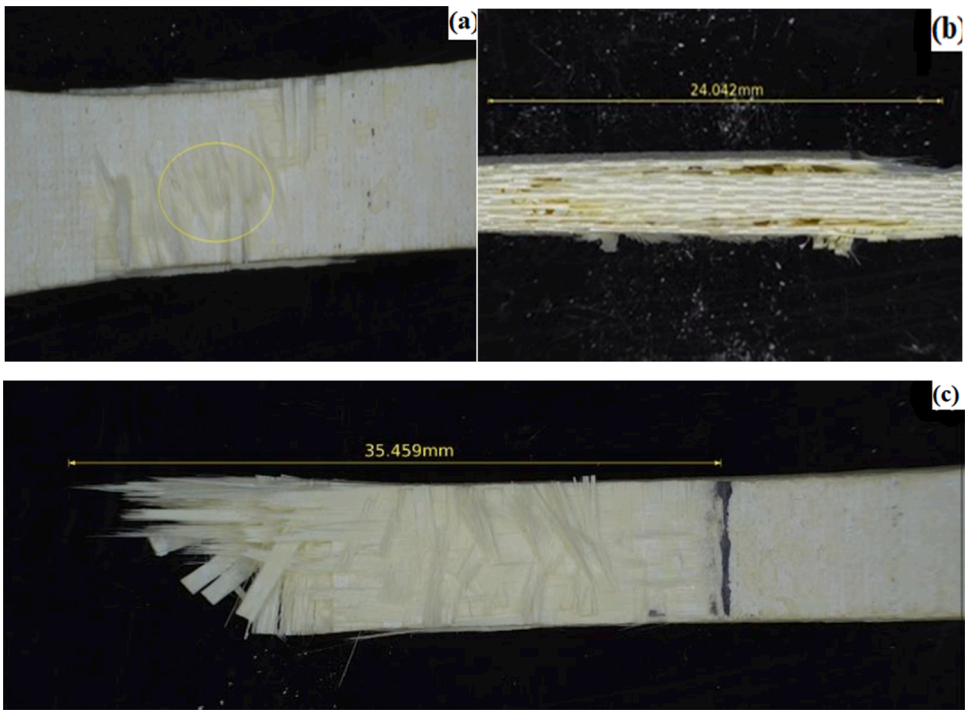

Fig. 12. (a) Twisting effect on neck mid region of sample (b) Delamination at first and bottom layer of oxide CMC and (c) Fibre pull-out along opposite direction of stress on laminar notched sample.

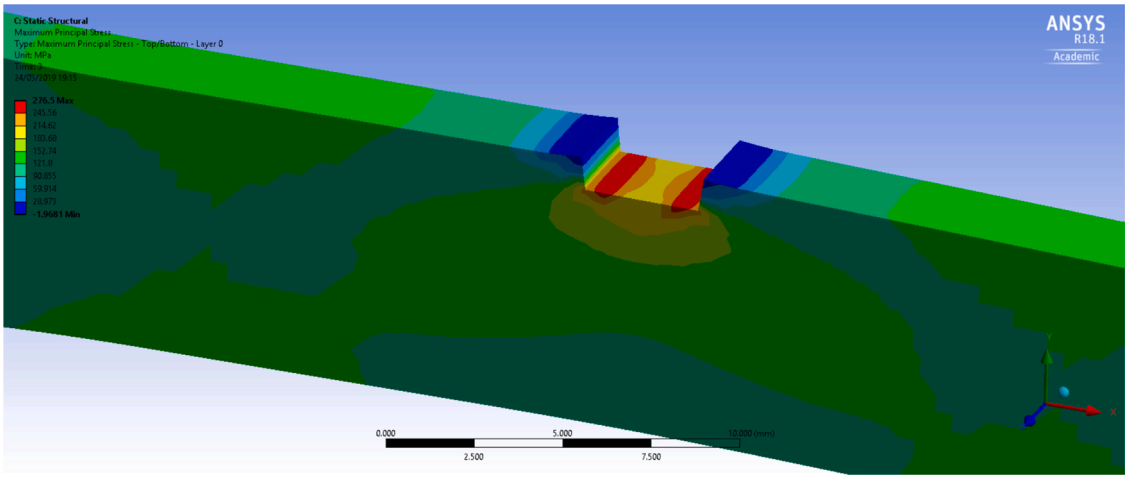

Fig. 13. Shear Stress concentration on the edges of laminar notches at 1000 °C.

debonding and fibre pull-out deactivation which results in catastrophic failure of the CMC [29]. This failure was observed for the lateral and double notched samples with the transfer of twisting stress into the shear stress which resulted in dynamic failure in the CMC samples.

Computational method was carried out to study the effect of notches at high temperatures of 900−1100 °C. The inputs for computational model were from the results obtained from unnotched high temperature samples. Even through the deformation on the samples were not the priority of validation, the computational method was utilised to view the effect of shear stress acting on the notches which could be considered as a reason for failure of CMC at high temperature. By observing the shear stress on all the three different temperatures it reveals that maximum stress is concentrated on the edges of the notches with further transfer of the stress towards the top of the surface as shown in Fig. 13. This concentration of shear stress justifies the delamination occurring on the first layers of the CMC along with formation of twists on the surfaces of midplanes.

Ambient condition fatigue test was also carried out for notched samples with the same conditions as of unnotched CMCs. Total of 5 double notched samples were tested with the same % UTS values of that of unnotched samples. Fig. 9 shows the SN curve for the notched and unnotched samples. From the Fig. 9, it can be said that samples with higher % UTS had the lowest resistance to cyclic fatigue load whereas samples with lower UTS % load was able to hold for longer cycles. Sample with lower fatigue load was able to withstand 800,504 cycles which could be stated as endurance limit of the CMC with notches. While comparing the results with unnotched samples, the sample with lowest stress was able to withstand one million cycles without any fracture whereas in case of notched sample was only able to withstand 800,504 cycles. This severe reduction on the fatigue strength could be due to the lower fracture toughness and higher notch sensitivity of the CMCs [28].

By examining the failure on the CMCs, the samples with higher notch

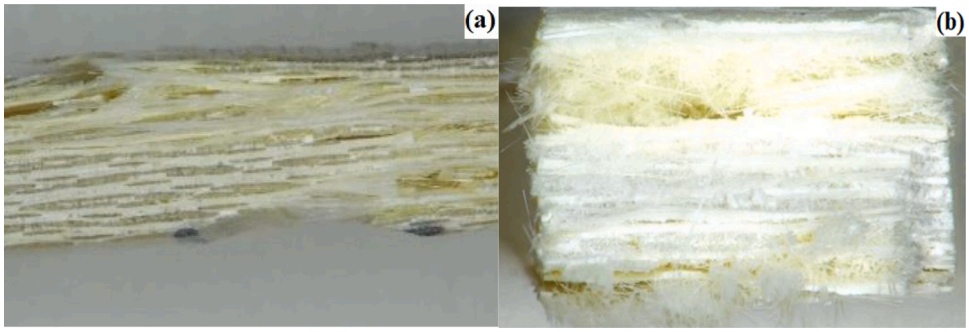

Fig. 14. (a) Buckling occurring on notched sample and (b) Fiber pull-out and delamination on top of surface.

sensitivities fractured due to two different failure mechanisms i.e., buckling and fibre-matrix debonding along with slighter effects from matrix cracking and fibre pull-out mechanisms whereas in case of less notch sensitive CMCs, the fracture was caused by delamination occurring due to matrix cracking. In high notch sensitive CMCs, the fatigue life was lesser than 200 cycles due to higher tensile load/stress acting on the surfaces. The buckling was the major phenomenon which led to delamination and debonding on the CMC owing to the compressive strength acting on the samples during fatigue cycle. The fracture planes also shown reasonable longer fibre pull-out along the mid plane due to the cyclic loading with matrix cracking followed by back-and-forth movement of fibres which resulted in the fibre sliding under load leading to fibre pull-out and debonding [30]. Delamination was observed on certain samples along with fibre pull-out mechanism due to deficit in fatigue strength by twist stress, shear stress acting along the mid plane and longer fibre pull-out at mid planes. The damage in mid plane without any delamination or fibre pull out in first plane may be due to the matrix cracks which could have observed stress concentrating leaving the top surface with lower stress level as shown in Fig. 14.

4. Conclusion

The present study focused on analysing the failure mechanisms of AS-N610 oxide-oxide CMCs under different thermo-mechanical conditions. The CMC exhibits high tensile strength (~430 MPa) at room temperature with fibre breaking and debonding being the two main degradation mechanisms by maximum damage occurring on the shoulders of the CMCs. The finite element model using ANSYS provided an evidence of shear stress distribution at the shoulders which justified the fracture behaviour. The thermal shock study at three different temperatures resulted in ~10 % deterioration in the tensile strength at 1100 °C due to release of thermal stresses, while in high temperature environment there was a rapid decline in tensile strength by nearly ~53 % for 1100 °C due to fibre pull-out acting normal to the fibre orientation. However, under tensile testing conditions the laminar notched samples represented a pseudo ductile behaviour with closer elastic modulus of unnotched samples and decreased tensile strength whereas lateral and double notched samples shown perfect brittle behaviour with increased elastic modulus (~20 %) and 30 % loss in tensile strength with fibre pull-out acting as the major fracture mechanism. The ambient condition fatigue test revealed that the CMC has an estimated service life of 1 million cycles under low cyclic load without any fracture. But with increase in cyclic load led to drastic loss in the fatigue life owing to delamination and fibre debonding mechanisms. The pre-manufactured notches also had impact in the service life by reducing the overall to 800,000 cycles for low cyclic load and less than 100 cycles for higher cyclic loads.

The study concluded that the fibre pull-out and delamination as the key mechanisms which decide the strength and service life of AS-N610. The material was able to sustain a temperature of 1100 °C with lesser decline in strength and service life of 1 million cycles at room temperature but the notch had a greater impact on the service and strength of material.

Funding and Acknowledgement

Authors would like to thank Dr Anish Paul, Ansaldo Energia, Switzerland for providing oxide CMC samples for research. The authors acknowledge the support of Mr. Dean Wells and Mr. Alex Vine from Kingston University, London and Mr. Collin Small and Mr. Martin Bache from Swansea University for their assistance offered towards mechanical testing. One of the authors, Karthikeyan would like to acknowledge the support provided by Kingston University, London for the studentship towards his PhD research.

Declaration of Competing Interest

The authors declare that they do not have any known competing financial or personal relationship that could have appeared to influence the work in the paper.

References

[1] K. Chawla, Ceramic Matrix Composites, Springer Science & Business Media, 2013.
[2] H. Ohnabe, S. Masaki, M. Onozuka, K. Miyahara, T. Sasa, Potential application of ceramic matrix composites to aero-engine components, Compos. Part A Appl. Sci. Manuf. 30 (4) (1999) 489–496.
[3] D. Desimone, D. Jayaseelan, W. Lee, A. Boccaccini, Development of ZrO2 interfaces for all-oxide composites, Compos. Sci. Technol. 72 (2) (2012) 197–203.
[4] K. Niihara, New design concept of structural ceramics, J. Ceram. Soc. Jpn. 99 (1154) (1991) 974–982.
[5] K. Ramachandran, R. Subramani, T. Arunkumar, V. Boopalan, Mechanical and thermal properties of spark plasma sintered Alumina-MWCNTs nanocomposites prepared via improvised colloidal route, Mater. Chem. Phys. 272 (125034) (2021).
[6] W. Krenkel, Carbon Fiber reinforced CMC for high-performance structures, Int. J. Appl. Ceram. Technol. 1 (2) (2004) 188–200.
[7] M.H. Lewis, A. Tye, E.G. Butler, P.A. Doleman, Oxide CMCs: interphase synthesis and novel fibre development, J. Eur. Ceram. Soc. 20 (5) (2000) 639–644.
[8] D. Salvo, E.E. Sackett, R. Johnston, D. Thompson, P. Andrews, M. Bache, Mechanical characterisation of a fibre reinforced oxide/oxide ceramic matrix composite, J. Eur. Ceram. Soc. 35 (16) (2015) 4513–4520.
[9] C.G. Levi, J.Y. Yang, B.J. Dalgleish, F. W.Zok, A.G. Evans, Processing and performance of an all-oxide ceramic composite, J. Am. Ceram. Soc. 81 (8) (1998) 2077–2086.
[10] S. Hackemann, F. Flucht, W. Braue, Creep investigations of alumina-based all-oxide ceramic matrix composites, Compos. Part A Appl. Sci. Manuf. 41 (12) (2010) 1768–1776.
[11] J. Chermant, G. Boitier, S. Darzens, G. Farizy, J. Vicens, J. Sangleboeuf, The creep mechanism of ceramic matrix composites at low temperature and stress, by a material science approach, J. Eur. Ceram. Soc. 22 (14-15) (2002) 2443–2460.
[12] D. Wilson, L. Visser, High performance oxide fibers for metal and ceramic composites, Composites Part A: Appl. Sci. Manufacturing 32 (8) (2001) 1143–1153.
[13] J. Goldsby, H. Yun, G. Morscher, J. Diacarlo, Annealing effects on creep of polycrystalline alumina-based fibers, Mater. Sci. Eng. A 242 (1-2) (1998) 278–283.
[14] C. Kastritseas, P.A. Smith, J.A. Yeomans, Thermal shock fracture in unidirectional fibre-reinforced ceramic–matrix composites, Compos. Sci. Technol. 65 (11-12) (2005) 1880–1890.
[15] D.M. Wilson, Statistical tensile strength of NextelTM 610 and NextelTM 720 fibres, J. Mater. Sci. 32 (10) (1997) 2535–2542.

[16] D.M. Wilson, D.C. Lueneburg, S.L. Lieder, High Temperature Properties of Nextel 610 and Alumina-based Nanocomposite Fibers, in John Wiley & Sons InC, 1993.
[17] E. Volkmann, K. Tushtev, D. Koch, C. Wilhelmi, J. Goring, K. Rezwan, Assessment of three oxide/oxide ceramic matrix composites: mechanical performance and effects of heat treatments, Compos. Part A Appl. Sci. Manuf. 68 (2015) 19–28.
[18] A. C1359-11, Standard Test Method for Monotonic Tensile Strength Testing of Continuous Fiber-Reinforced Advanced Ceramics With Solid Rectangular Cross-Section Test Specimens at Elevated Temperatures, ASTM International, West Conshohocken, PA, 2011.
[19] Ansys®, "Academic Research Mechanical, Release 18.1," Ansys, Inc.
[20] A.K. Singh, V. Sabelkin, S. Mall, Fatigue behavior of double-edge notched oxide/oxide ceramic matrix composite in a combustion environment, J. Compos. Mater. 51 (26) (2017) 3669–3683.
[21] R.A. Simon, Progress in processing and performance of porous-matrix Oxide/Oxide composites, Int. J. Appl. Ceram. Technol. 2 (2) (2005) 141–149.
[22] C.G. Levi, J.Y. Yang, B.J. Dalgleish, F.W.a.A.G. Evans, Processing and performance of an all-oxide ceramic composite, J. Am. Ceram. Soc. 81 (8) (1998) 2077–2086.
[23] Z. Yang, H. Yuan, H. Liu, Evolution and characterization of cyclic thermal shock-induced thermomechanical damage in oxide/oxide ceramics matrix composites, Int. J. Fatigue 120 (2019) 150–161.
[24] Z. Yang, H. Yuan, B. Markert, Representation of micro-structural evolution and thermo-mechanical damage in thermal shocked oxide/oxide ceramic matrix composites, Int. J. Fatigue 126 (2019) 122–129.
[25] G. Fantozzi, P. Reynaud, Mechanical hysteresis in ceramic matrix composites, Mater. Sci. Eng. A 521-522 (2009) 18–23.
[26] V. Kramb, R. John, L. Zawada, Notched fracture behaviour of an oxide/oxide ceramic-matrix composite, J. Am. Ceram. Soc. 82 (11) (1999) 3087–3096.
[27] P. Spriet, CMC applications to gas turbines. in Ceramic Matrix Composites: Materials, Modeling and Technology, Wiley, 2015, pp. 591–608.
[28] P. Mallick, Fiber-Reinforced Composites: Materials, Manufacturing, and Design, third edition, CRC Press, 2008.
[29] D. Zhang, D. Hayhurst, Stress–strain and fracture behaviour of 0/90 and plain weave ceramic matrix composites from tow multi-axial properties, Int. J. Solids Struct. 47 (21) (2010) 2958–2969.
[30] L. Longbiao, Micromechanical modeling for tensile behaviour of carbon Fiber – reinforced ceramic – matrix composites, Appl. Compos. Mater. 22 (2015) 773–790.